Structuring of polymer solutions upon solvent evaporation

C. Schaefer,[1,2,*] P. van der Schoot,[2] and J. J. Michels[3,†]
[1]*Dutch Polymer Institute, P.O. Box 902, 5600 AX Eindhoven, The Netherlands*
[2]*Theory of Polymers and Soft Matter, Eindhoven University of Technology, P.O. Box 513, 5600 MB Eindhoven, The Netherlands*
[3]*Holst Centre/TNO, High Tech Campus 31, 5656 AE Eindhoven, The Netherlands*
(Received 25 July 2014; revised manuscript received 30 September 2014; published 18 February 2015)

The morphology of solution-cast, phase-separated polymers becomes finer with increasing solvent evaporation rate. We address this observation theoretically for a model polymer where demixing is induced by steady solvent evaporation. In contrast to what is the case for a classical, thermal quench involving immiscible blends, the spinodal instability initially develops slowly and the associated length scale is not time invariant but decreases with time as $t^{-1/2}$. After a time lag, phase separation accelerates. Time lag and characteristic length exhibit power-law behavior as a function of the evaporation rate with exponents of $-2/3$ and $-1/6$. Interestingly, at later stages the spinodal structure disappears completely while a second length scale develops. The associated structure coarsens but does not follow the usual Lifshitz-Slyozov-Wagner kinetics.

DOI: 10.1103/PhysRevE.91.022602 PACS number(s): 82.35.Lr, 61.25.he, 64.75.St, 81.15.Aa

The properties of high-performance polymeric materials can be tuned by blending immiscible molten polymers [1,2]. Such materials have morphologies with nano- or microscale features. Depending on the mixing ratio of the constituents, bicontinuous or droplet morphologies result that are frozen in upon solidification. Similar structures spontaneously appear in binary polymer mixtures following a temperature quench into the miscibility gap of the phase diagram [2]. Quenching allows for some control over the morphology because the quench depth dictates the predominant length scale of the structure prior to coarsening. For thin-film applications such as in organic photovoltaics [3], organic memory diodes [4], and membrane technology [5], however, casting the blend from a low-molecular-weight solvent is strongly preferred over melt processing. The quench is in that case a concentration quench, albeit the mean concentration increases during the demixing due to ongoing evaporation [6]. Here we show theoretically that for a polymer-solvent mixture steady evaporation drastically changes the demixing kinetics, giving rise to multiple length scales that have also been observed experimentally.

Phase separation induced by solvent evaporation has been extensively studied, often involving spin coating [7–12] as it provides excellent control over evaporation and hence the quench rate [13–15]. Experimental and theoretical studies have shown that upon fast evaporation a blend demixes along concentration gradients perpendicular to the substrate or liquid-gas interface, i.e., in a stratified fashion. This results in a layered morphology, consisting of lamellar domains that may subsequently break up into lateral features [16–18]. Whether the stratified morphology is retained in the dry film depends on the demixing kinetics. A numerical study has shown that for slow evaporation and weak surface interaction stratification becomes less important and thin-film phase separation is bulk-like [17]. Indeed, blend solutions have been reported for which no stratified regime could be identified [15].

In addition to the insight into stratification, experimental studies have also demonstrated that average domain size decreases with evaporation rate [7]. Qualitatively, this trend has been attributed to shortening of the time available for coarsening of the morphology prior to solidification [7,11]. In fact, time-resolved *in situ* microscopy shows that the evaporation rate also influences the emerging predominant length scale [11], as faster evaporation results in a deeper quench into the miscibility gap, leading to a smaller length scale that survives coarsening. Furthermore, several other studies point at the emergence of a second, nonspinodal length scale that develops after initial demixing [9,10]. At present, no theoretical study describes and explains how solvent evaporation affects the appearance and development of structural length scales.

To account for this hiatus, we address phase separation in polymer solutions by invoking a generalized diffusion equation extended to allow for evaporation. For simplicity we do not consider binary polymer mixtures but restrict ourselves to a single polymer in solution. The latter is analytically much more tractable owing to the drastically reduced number of parameters. As we will show in follow-up work, the early stages of demixing of our model polymer solution are identical to those in binary polymer solutions and the conclusions we draw for the single-polymer carry over to blends [19].

Our evaluation of the diffusion equation shows that evaporation drastically changes conventional phase-separation kinetics. At early stages of demixing, under steady evaporation the dominant length scale of a spinodally demixing solution decreases with time as $t^{-1/2}$, up to a characteristic time that is determined by the evaporation rate, solvent quality, diffusivity, and concentration. At intermediate stages, a second length scale appears that grows due to coarsening, strikingly not obeying the classical Lifshitz-Slyozov-Wagner power law. In the late stages redissolution kinetics takes over when crossing the high-concentration binodal.

We model phase separation of a polymer solution in a d-dimensional volume by letting chemical potential gradients drive diffusive transport. The chemical potential is the functional derivative $\delta\mathcal{F}/\delta\phi$ of the free energy $\mathcal{F}[\phi]$ with respect to the polymer volume fraction ϕ. Here and below we use

*c.schaefer@tue.nl
†Present address: Max Planck Institute for Polymer Research, Ackermannweg 10, 55128 Mainz, Germany.

units of thermal energy. The free energy is the volume integral $\mathcal{F}[\phi] = \frac{1}{a^d}\int dV(f_{\rm loc} + f_{\rm nonloc})$ of the sum of a local and a nonlocal free energy per segment volume a^d, $f_{\rm loc}$ and $f_{\rm nonloc}$. For the former, we invoke a Flory-Huggins free energy density $f_{\rm loc}(\phi) = \phi\ln\phi/N + (1-\phi)\ln(1-\phi) + \phi(1-\phi)\chi$, where χ is the Flory interaction parameter and N is the polymer chain length in number of segments. For $\chi > \frac{1}{2}(1+1/\sqrt{N})^2$ the solvent quality is low and the polymer phase separates if the concentration is in between the high- and low-concentration branches of the binodal [20]. The nonlocal contribution to the free energy penalizes concentration gradients and is of the usual form $f_{\rm nonloc} = \frac{1}{2}\kappa|\nabla_{\mathbf{r}}\phi|^2$ [21,22], with a "stiffness" κ that we take as a free model parameter. The tacit assumption is that concentration gradients are weak on the scale of the size of the chains so that the concentration dependence of κ due to chain statistics is unimportant [23].

In the conventional case, where the polymer solution is temperature quenched into the spinodal region, phase-separation kinetics can be described by $\partial_t\phi = \nabla_{\mathbf{r}}\cdot[\phi D\nabla_{\mathbf{r}}\delta\mathcal{F}/\delta\phi] + \eta$. Here, $\phi = \phi(\mathbf{r},t)$ denotes a local polymer volume fraction that depends on position $\mathbf{r}$ and time t, ϕD the slow-mode mobility in case the solvent is much more mobile than the polymer [24], and η a noise term accounting for thermal fluctuations. The Gaussian stochastic variable η is δ-correlated in time and has zero mean and covariance: $\langle\eta(\mathbf{r}',t')\eta(\mathbf{r},t)\rangle = -2\phi D\nabla^2_{\mathbf{r}}\delta(\mathbf{r}'-\mathbf{r})\delta(t'-t)$ [21,25]. The early-time solution of this equation gives for the fastest growing unstable mode $q_* = \sqrt{-\partial_{\phi\phi}f_{\rm loc}/2\kappa}$, which characterizes the emerging morphology. The rate of the fastest growing density modulation obeys $|R| = Da^{-d}\phi\kappa q_*^4$, where ϕ denotes the mean polymer concentration [21,22].

In our case, the "quench" is isothermal and driven by steady evaporation; i.e., the local concentration increases as $\phi(\mathbf{r},t) = \phi_0 + \int dt\alpha$, such that the mixture becomes gradually thermodynamically unstable as the mean polymer concentration crosses the spinodal concentration ϕ_0. Here, the coefficient α plausibly depends on the local concentration and hence on time [13]. If the evaporation rate is proportional to the surface concentration and if stratification is absent, then conservation of total volume gives $\alpha = k\phi^2(1-\phi)$ with k a proportionality coefficient that depends on vapor pressure, solvent quality, spin speed, etc. [13]. We note that the kinetics due to evaporation differs from that of a system in which one component is converted into the other by irreversible first order reaction. In that case one would expect α to be proportional with $k(1-\phi)$, where k now represents a reaction rate constant. For short times, we may either insert $\phi = \phi_0$ in the expression for α or pre-average over α, yielding $\phi = \phi_0 + \alpha t$. The "evaporation rate" α then becomes time independent, and we also take it as a free parameter. Experimentally, the mean value of α can be controlled, e.g., via the spin speed [7,10,11].

In what follows, we focus on systems for which stratification is of minor importance [15,17], owing to (i) weak interface adsorption and (ii) diffusion counteracting accumulation of material near the surface due to evaporation. The latter is valid as long as the Biot number, $\mathrm{Bi} = \alpha h_0^2/\phi Da^{-d}\partial_{\phi\phi}f_{\rm loc}$, with h_0 the initial layer thickness and $\phi Da^{-d}\partial_{\phi\phi}f_{\rm loc}$, the collective diffusivity, is much smaller than unity [17]. Hence, for computational convenience, we model our system as (quasi-)two-dimensional, so $d = 2$.

Within this description, the relevant diffusion equation becomes

$$\partial_t\phi = \nabla_{\mathbf{r}}\cdot\left[\phi D\nabla_{\mathbf{r}}\frac{\delta\mathcal{F}}{\delta\phi}\right] + \alpha + \eta, \qquad (1)$$

where evaporation acts as a source term for polymeric material. To enhance analytical tractability, we presume the diffusivity D to be concentration independent. Typically the metastable region is traversed owing to fast evaporation, so that demixing starts in the spinodal region, where the solution is thermodynamically unstable. Hence, at $t = 0$, we take for the uniform volume fraction ϕ_0 a value from the low-concentration branch of the spinodal, described by the condition $\partial_{\phi\phi}f_{\rm loc} = 0$. These initial conditions allow the system to become gradually instable as evaporation proceeds. Our approach is dedicated to rigorous analysis of the case of evaporation and, for that, markedly different from any system in which demixing relies on an instantaneous quench into the instable region. In particular, we emphasize the difference between our approach and that of Glotzer *et al.*, who consider the coupling between a reversible reaction and phase separation upon quenching into the spinodal region. In contrast, in our case evaporation is irreversible and demixing starts at the spinodal line [26].

We solve Eq. (1) for a host of values of interaction parameter χ, degree of polymerization, N, and evaporation rate α. For this we rely on a finite difference scheme on a 512×512 square grid, invoking adaptive [16] explicit Euler time steps and central differences in position. At $t = 0$ the mixture is homogeneous, and for $t > 0$ concentration fluctuations are implemented at each time step via the method introduced in Ref. [27].

Representative morphology images obtained at different times for $\chi = 1.0$, $N = 10$, and dimensionless evaporation rate (defined below) of $\tilde{\alpha} = 5.5\times10^{-4}$ are shown in Fig. 1. After entering the spinodal, concentration variations remain small up to a "lag time," $\tau_{\rm L}$, that we also specify below. After that time a convoluted lamellarlike texture appears that subsequently coarsens. In the late stages, this structure breaks up into droplets devoid of polymer in a polymer-rich matrix.

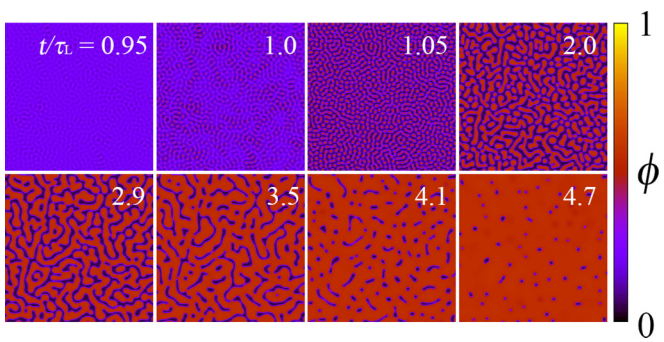

FIG. 1. (Color online) Evaporation-induced structure development in a polymer solution, for interaction parameter $\chi = 1.0$, degree of polymerization, $N = 10$, and evaporation rate $\tilde{\alpha} = 5.5\times10^{-4}$ scaled to the diffusion time scale. The color (gray scale) coding indicates differences in polymer volume fraction ϕ. At a lag time $t = \tau_{\rm L}$ (see main text), a phase-separated structure becomes discernible (see also Figs. 2 and 3).

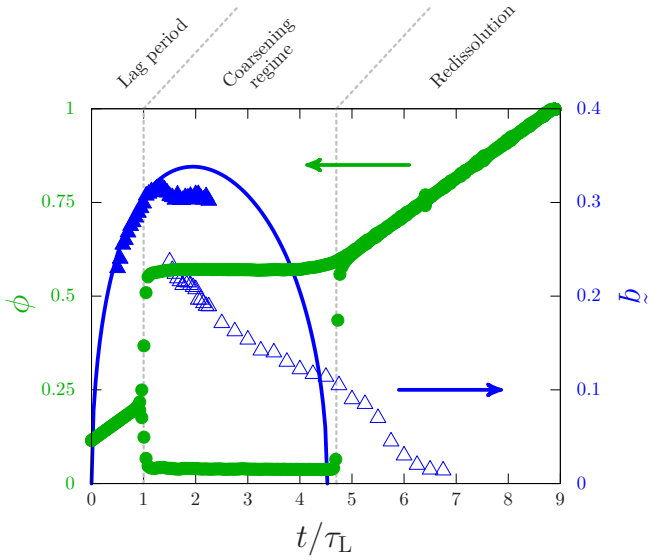

FIG. 2. (Color online) The volume fraction, ϕ, indicated on the left vertical axis in green (light gray) and dimensionless wave number, $\tilde{q}$, indicated on the right in red (dark gray), as a function of time t relative to the lag time τ_L for the parameter values in Fig. 1. The spinodal is crossed at $t = 0$, for $t/\tau_L \approx 1$ the binodal concentrations are approached (solid circles), and the structure coarsens. At $t/\tau_L \approx 4.8$ the high-concentration branch of the binodal is reached by evaporation and the polymer redissolves. The morphology is initially characterized by a wave number (solid triangles) predicted from linearized theory in Eq. (3) (line). After the lag time a new length scale appears (open triangles).

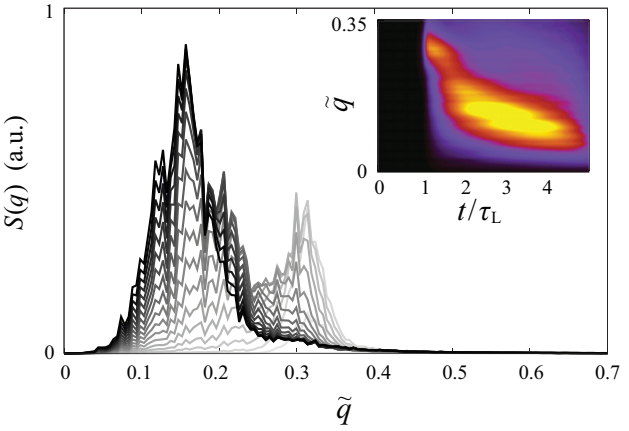

FIG. 3. (Color online) Structure factor, $S(q)$, for different times running from $t/\tau_L = 0$ (light grey) to $t/\tau_L = 4.5$ (black) corresponding to Figs. 1 and 2. The inset highlights the subsequent appearance and disappearance of two structure peaks.

In Fig. 2, we analyze the structures of Fig. 1 in terms of a predominant wavelength, as well as the concentrations in the polymer-rich and polymer-poor regions. Focusing on the latter first, we observe that after entering the spinodal region at $t = 0$, the density remains nearly uniform, demonstrating that initially spinodal decomposition is slow. The reason is that the driving force for phase separation remains weak and that the relevant spinodal length scale is large, requiring mass to be transported over large distances. Composition bifurcation takes place after the lag time, τ_L, which is not to be confused with the lag time from nucleation theory [28]. Within a very short period following τ_L, the concentrations in the two coexisting phases approach the corresponding binodal values. Once the mean concentration reaches the high-concentration branch of the binodal, redissolution occurs (at $t/\tau_L \approx 4.8$ in Fig. 2).

Focusing now on the structure development, we find that the predominant wave number first increases and subsequently decreases with time. The initial increase for $t < \tau_L$ is caused by evaporation driving the system deeper into the unstable region. Strikingly, at the point where the initial predominant wave number starts to decrease slowly, a second, significantly larger length scale appears at the expense of the first. This second length scale represents the structure that eventually coarsens. For a relatively small period of time the two length scales coexist, which is demonstrated more clearly by the evolution of the structure factor $S(q)$ in Fig. 3. We find that this unusual kinetics carries over to binary polymer solutions and hence seems to be universal and directly linked to evaporation predominating over diffusive mass transport [19]. As mentioned, the appearance of a second peak has indeed been observed experimentally in solution-cast macromolecular blends but is typically not encountered during conventional temperature quench-type spinodal decomposition in the absence of evaporation [9,10]. Whether the second length scale emerging from the numerical calculations is indeed the same as the one observed in experimental systems is currently under investigation.

From our numerical calculations we have found that after spinodal decomposition the phase-separated structure, represented by this second length scale, typically coarsens with a rate different from that predicted by the Lifshitz-Slyozov-Wagner theory that states that the relevant length scale grows with an exponent of $1/3$, independent of dimensionality [22]. For very slow evaporation we retrieve this power law, whereas for fast evaporation the exponent tends to a value of $1/2$, pointing at a different coarsening mechanism. Indeed, if we (i) ignore diffusion and focus entirely on the effects of evaporation, (ii) presume the concentration of polymer in the dense domains to be very near the binodal value (see Fig. 2), and (iii) invoke mass conservation, we find that evaporation should lead to a power law with exponent $1/d$, with d the dimensionality of space. So, for $d = 2$ we indeed retrieve the observed scaling exponent. This suggests that the second length scale originates from the tendency of high-concentration domains to reach beyond the binodal value under the action of evaporation. A second length scale originating from purely diffusive dynamics is an interesting feature, as the phenomenon has also been suggested to result from capillarity-driven flow [9].

At the stage where the mean concentration becomes virtually equal to the binodal value, redissolution commences. In this regime the dominant length scale further increases at an even stronger time dependence that appears to be a function of the evaporation rate. Eventually, all structure disappears. Obviously, for a binary polymer solution that phase-separates upon solvent evaporation this last regime does not occur.

The fact that for times smaller than the lag time, $t < \tau_L$, the concentration variations remain small allows us to calculate the time dependence of the wave number of the spinodal mode as well as the lag time from a linearized version of the theory. Fourier transformation of the resulting linearized diffusion equation yields an ordinary differential equation, the solution of which we cast in the usual form:

$$\ln \delta\hat{\phi}(q,t)/\delta\hat{\phi}(q,0) = -R(q,t)t, \tag{2}$$

with $R(q,t) = (q^2 D/a^2 t)\int_0^t dt'[\phi(t')\partial_{\phi\phi} f_{\rm loc}(\phi(t')) + q^2\phi(t')\kappa]$ the relaxation rate, now time dependent due to evaporation [21,22]. By setting $\partial R(q,t)/\partial q = 0$, we obtain the time-dependent predominant wave number,

$$q_*^2(t) = -\int_0^t dt'\phi(t')\partial_{\phi\phi} f_{\rm loc}(\phi(t'))/2\kappa \int_0^t {\rm d}t''\phi(t''), \tag{3}$$

where $\phi(t) = \phi_0 + \alpha t$, with ϕ_0 the concentration at which we enter the spinodal region. Figure 2 shows that for $t < \tau_L$ this prediction excellently agrees with our numerical results. As expected, for $t > \tau_L$ the prediction fails.

We calculate the lag time, τ_L, by inserting $q = q_*$ and $t = \tau_L$ into $R(q_*(t),t)$ and Eq. (2), and solve

$$\ln r_L = a^{-2}\kappa D(\phi_0 + \alpha\tau_L/2)q_*^4(\tau_L)\tau_L. \tag{4}$$

The fact that τ_L is a weak function of the amplitude of the concentration fluctuation at the lag time relative to that at time zero, $r_L \equiv \delta\hat{\phi}(q_*(\tau_L),\tau_L)/\delta\hat{\phi}(q_*(\tau_L),0)$, which we show later, allows us to quantify τ_L by using r_L as a free parameter to fit Eq. (4) to our numerical results. Subsequently, we insert the lag time so obtained into Eq. (3) to obtain the predominant wave number at the lag time.

The excellent agreement between our analytical estimate and the numerical results is shown in Fig. 4. In the figure, we scale the wave number, the lag time, and the evaporation rate appropriately to produce dimensionless quantities. To render the wave number dimensionless, we multiply it by the square root of the stiffness, $\tilde{q}_* \equiv \sqrt{\kappa}q_*$. We scale the lag time and evaporation rate to two different natural time scales that we obtain by linearizing Eq. (4) to yield $\tau_L^3 = 16(\kappa a^2/\phi_0 D)(\partial_{\phi\phi\phi} f_{\rm loc}(\phi_0)\alpha)^{-2}\ln r_L$, which indeed shows that τ_L is a weak function of r_L. From this, we read off a natural time scale measuring the rate at which the polymer solution destabilizes due to evaporation, $\tau_e \equiv 1/|\partial_{\phi\phi\phi} f_{\rm loc}(\phi_0)\alpha|$, and one for self-diffusion $\tau_d \equiv \kappa a^2/\phi_0 D$. This result allows us to define scaled parameters $\tilde{\alpha} \equiv \tau_d/\tau_e$ and $\tilde{\tau}_L \equiv \tau_L/\tau_d$ as well as universal scaling relations for the lag time,

$$\tau_L \approx \tau_e^{2/3}\tau_d^{1/3} \propto \alpha^{-2/3}, \tag{5}$$

and predominant wave number at the lag time,

$$q_*(\tau_L) \approx \kappa^{-1/2}(\tau_d/\tau_e)^{1/6} \propto \alpha^{1/6}, \tag{6}$$

where in the first approximate equalities we ignore a prefactor of order unity. These scaling relations show how lag time and emerging morphology universally depend not only on evaporation rate, but also on the two fundamental time scales of the problem, one set by diffusion and the other by the skewness of the free energy near the spinodal.

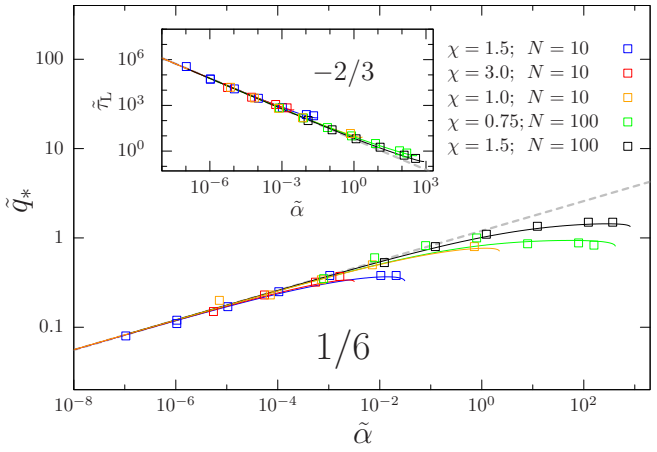

FIG. 4. (Color online) The dimensionless predominant wave number $\tilde{q}_*$ (main figure) and lag time $\tilde{\tau}_L$ (inset) as a function of the dimensionless evaporation rate $\tilde{\alpha}$ for various interaction parameter values χ and degree of polymerization, N. The numerical (symbols) results are curve fitted from linearized theory (solid lines) and approach limiting power laws (dashed lines) for slow evaporation.

In conclusion, we have shown that evaporation drastically changes the spinodal decomposition of a polymer solution, as compared to classical temperature-quenched systems. For short times upon entering the spinodal region, the thermodynamic driving force is weak and the unstable wavelength large, implying very slow demixing. The predominant wavelength decreases in time owing to ongoing evaporation that further destabilizes the solution. This sets a lag time after which phase separation accelerates and the wavelength saturates. Subsequently, a second length scale appears during which the original spinodal mode disappears. This second length scale describes a structure that coarsens, not following the classical Lifshitz-Slyozov-Wagner power law. Once the mean concentration approaches the binodal, a third, much faster, kinetic regime sets in where redissolution takes place. Our study demonstrates that the evaporation rate crucially influences morphology and that a quantitative understanding of this dependence is of essential importance to the controlled production of thin-film devices and membranes.

This research forms part of the research program of the Dutch Polymer Institute (DPI), Project No. 734. The authors thank M. A. J. Michels and J. J. van Franeker for useful discussions.

[1] F. W. Billmeyer, Jr., *Textbook of Polymer Science*, 3rd ed. (John Wiley and Sons, New York, 1984).

[2] L. H. Sperling, *Introduction to Physical Polymer Science*, 4th ed. (John Wiley and Sons, Hoboken, NJ, 2006).

[3] A. J. Moulé and K. Meerholz, Morphology control in solution-processed bulk-heterojunction solar cell mixtures, Adv. Funct. Mater. **19**, 3028 (2009); C. J. Brabec, S. Gowrisanker, J. J. M. Halls, D. Laird, J. Jia, and S. P. Williams, Polymerfullerene bulk-heterojunction solar cells, Adv. Mater. **22**, 3839 (2010); F. Liu, Y. Gu, J. W. Jung, W. H. Jo, and T. P. Russell, On the morphology of polymer-based photovoltaics, J. Polym. Sci. B: Polym. Phys. **50**, 1018 (2012).

[4] K. Asadi, D. M. de Leeuw, B. de Boer, and P. W. M. Blom, Organic non-volatile memories from ferroelectric phase-separated blends, Nat. Mater. **7**, 547 (2008); K. Asadi, H. J. Wondergem, R. S. Moghaddam, C. R. McNeill, N. Stingelin, B. Noheda, P. W. M. Blom, and D. M. de Leeuw, Spinodal decomposition of blends of semiconducting and ferroelectric polymers, Adv. Funct. Mater. **21**, 1887 (2011); M. Li, N. Stingelin, J. J. Michels, M. J. Spijkman, K. Asadi, R. Beerends, F. Biscarini, P. W. M. Blom, and D. M. de Leeuw, Processing and low voltage switching of organic ferroelectric phase-separated bistable diodes, *ibid.* **22**, 2750 (2012); V. Khikhlovskyi, R. Wang, A. J. J. M. van Breemen, G. H. Gelinck, R. A. J. Janssen, and M. Kemerink, Nanoscale organic ferroelectric resistive switches, J. Phys. Chem. C **118**, 3305 (2014).

[5] P. van de Witte, P. J. Dijkstra, J. W. A. van den Berg, and J. Feijen, Phase separation processes in polymer solutions in relation to membrane formation, J. Membr. Sci. **117**, 1 (1996); M. Ulbricht, Advanced functional polymer membranes, Polymer **47**, 2217 (2006); F. Liu, N. A. Hashim, Y. Liu, M. R. Moghareh Abed, and K. Li, Progress in the production and modification of PVDF membranes, J. Membr. Sci. **375**, 1 (2011).

[6] M. Sprenger, S. Walheim, A. Budkowski, and U. Steiner, Hierarchic structure formation in binary and ternary polymer blends, Interface Sci. **11**, 225 (2003).

[7] S. Waldheim, M. Böltau, J. Mlynek, G. Krausch, and U. Steiner, Structure formation via polymer demixing in spin-cast films, Macromolecules **30**, 4995 (1997); K. Dalnoki-Veress, J. A. Forrest, J. R. Stevens, and J. R. Dutcher, Phase separation morphology of spin-coated polymer blend thin films, Physica A **239**, 87 (1997); H. Zhang and S. Takeoka, Morphological evolution within spin-cast ultrathin polymer blend films clarified by a freestanding method, Macromolecules **45**, 4315 (2012); S. Kouijzer, J. J. Michels, M. van den Berg, V. S. Gevaerts, M. Turbiez, M. M. Wienk, and R. A. J. Janssen, Predicting morphologies of solution processed polymer:fullerene blends, J. Am. Chem. Soc. **135**, 12057 (2013).

[8] J. Bergqvist, S. A. Mauger, K. Tvingstedt, H. Arwon, and O. Inganäs, *In situ* reflectance imaging of organic thin film formation from solution deposition, Sol. Energy Mater. Sol. Cells **114**, 89 (2013).

[9] S. Ebbens, R. Hodgkinson, A. J. Parnell, A. Dunbar, S. J. Martin, P. D. Topham, N. Clarke, and J. R. Howse, *In situ* imaging and height reconstruction of phase separation processes in polymer blends during spin coating, ACS Nano **5**, 5124 (2011).

[10] J. J. van Franeker, D. Westhoff, M. Turbiez, M. M. Wienk, V. Schmidt, and R. A. J. Janssen, Controlling the dominant length scale of liquid-liquid phase separation in spin-coated organic semiconductor films, Adv. Func. Mater. **25**, 855 (2015).

[11] D. T. W. Toolan, E. ul Haq, A. Dunbar, S. Ebbens, N. Clarke, P. D. Topham, and J. R. Howse, Direct observation of morphological development during the spin-coating of polystyrenepoly(methyl methacrylate) polymer blends, J. Polym. Sci. B. **51**, 875 (2013).

[12] P. C. Jukes, S. Y. Herlot, J. S. Sharp, and R. A. L. Jones, Time-resolved light scattering studies of phase separation in thin film semiconducting polymer blends during spin-coating, Macromolecules **38**, 2030 (2005).

[13] D. E. Bornside, W. W. Macosko, and L. E. Scriven, Spin coating of a PMMA/chlorobenzene solution, J. Electrochem. Soc. **138**, 317 (1991).

[14] A. Meyerhofer, Characteristics of resist films produced by spinning, J. Appl. Phys. **49**, 3993 (1978); D. E. Bornside, W. W. Macosko, and L. E. Scriven, Spin coating: Onedimensional model, *ibid.* **66**, 5185 (1989); D. B. Hall, P. Underhill, and J. M. Torkelson, Spin coating of thin and ultrathin polymer films, Polym. Eng. Sci. **38**, 2039 (1998); C. Chang, C. Pai, W. Chen, and S. A. Jenekhe, Spin coating of conjugated polymers for electronic and optoelectronic applications, Thin Solid Films **479**, 254 (2005); A. M. Münch, C. P. Please, and B. Wagner, Spin coating of an evaporating polymer solution, Phys. Fluids **23**, 102101 (2011).

[15] S. Nilsson, A. Bernasik, A. Budkowski, and E. Moons, Morphology and phase segregation of spin-casted films of polyfluorene/PCBM blends, Macromolecules **40**, 8291 (2007).

[16] O. Wodo and B. Genepathysubramanian, Computationally efficient solution to the CahnHilliard equation: Adaptive implicit time schemes, mesh sensitivity analysis and the 3D isoperimetric problem, J. Comp. Phys. **230**, 6037 (2011).

[17] O. Wodo and B. Genepathysubramanian, Modeling morphology evolution during solvent-based fabrication of organic solar cells, Comput. Mater. Sci. **55**, 113 (2012).

[18] P. Dayal and T. Kyu, Porous fiber formation in polymer-solvent system undergoing solvent evaporation, J. Appl. Phys. **100**, 043512 (2006); G. A. Buxton and N. Clarke, Ordering polymer blend morphologies via solvent evaporation, Europhys. Lett. **78**, 56006 (2007); P. Dayal, A. J. Guenthner, and T. Kyu, Morphology development of main-chain liquid crystalline polymer fibers during solvent evaporation, J. Polym. Sci. B. **45**, 429 (2007); A. J. Archer, M. J. Robbins, and U. Thiele, Dynamical density functional theory for the dewetting of evaporating thin films of nanoparticle suspensions exhibiting pattern formation, Phys. Rev. E **81**, 021602 (2010); Modelling the evaporation of thin films of colloidal suspensions using dynamical density functional theory, J. Phys. Condens. Matter **23**, 415102 (2011); A. Malijevský and A. J. Archer, Sedimentation of a two-dimensional colloidal mixture exhibiting liquid-liquid and gas liquid phase separation: A dynamical density functional theory study, J. Chem. Phys. **139**, 144901 (2013); J. J. Michels and E. Moons, Simulation of surface-directed phase separation in a solution-processed polymer/PCBM blend, Macromolecules **46**, 8693 (2013); S. Coveney and N. Clarke, Breakup of a transient wetting layer in polymer blend thin films: Unification with 1D phase equilibria, Phys. Rev. Lett. **111**, 125702 (2013); S. P. Paradiso, K. T. Delaney, C. J. García-Cervera, H. D. Ceniceros, and G. H. Fredrickson, Block copolymer self assembly during rapid solvent evaporation: Insights into cylinder growth and stability, ACS Macro Lett. **3**, 16 (2014).

[19] C. Schaefer, P. van der Schoot, and J. J. Michels (unpublished).

[20] P. J. Flory, Thermodynamics of high polymer solutions, J. Chem. Phys. **10**, 51 (1942); *Principles of Polymer Physics* (Cornell University Press, Ithaca, NY, 1953); P. J. Huggins,

Some properties of solutions of long-chain compounds, J. Phys. Chem. **46**, 151 (1942).

[21] J. W. Cahn and J. E. Hilliard, Free energy of a nonuniform system. I. Interfacial free energy, J. Chem. Phys. **28**, 258 (1958).

[22] J. D. Gunton, M. San Miguel, and P. S. Sahni, in *Phase Transitions and Critical Phenomena*, edited by C. Domb and J. L. Lebowitz (Academic, New York, 1983), Vol. 8.

[23] P. van der Schoot, Green-function description of dense polymeric systems, Macromolecules **33**, 8497 (2000).

[24] K. Binder, Collective diffusion, nucleation, and spinodal decomposition in polymer mixtures, J. Chem. Phys. **79**, 6387 (1983); F. Brochard, J. Jouffroy, and P. Levinson, Polymer diffusion in blends: Effects of mutual friction, Macromolecules **17**, 2925 (1984); P. G. de Gennes, Dynamics of fluctuations and spinodal decomposition in polymer blends, J. Chem. Phys. **72**, 4756 (1980).

[25] H. E. Cook, Brownian motion in spinodal decomposition, Acta Metall. **18**, 297 (1970); J. S. Langer, Theory of spinodal decomposition in alloys, Ann. Phys. **65**, 53 (1971); P. C. Hohenberg and B. I. Halperin, Theory of Critical Phenomena, Rev. Mod. Phys. **49**, 435 (1977).

[26] S. C. Glotzer, E. A. Di Marzio, and M. Muthukumar, Reaction-controlled morphology of phase-separating mixtures, Phys. Rev. Lett. **74**, 2034 (1995).

[27] R. G. Petschek and H. Metiu, A computer simulation of the time dependent Ginzburg-Landau model for spinodal decomposition, J. Chem. Phys. **79**, 3443 (1983).

[28] D. Kashchiev, *Nucleation: Basic Theory with Applications* (Butterworth-Heinemann, Oxford, 2000).